

Excitation, Impact and Control of Toroidicity-Induced Alfvén Eigenmodes in the JT-60U ICRF Experiments

KIMURA Haruyuki, SAIGUSA Mikio, KONDOH Takashi, OZEKI Takahisa,
MORIYAMA Shinichi and FUJII Tsuneyuki
*Naka Fusion Research Establishment, Japan Atomic Energy Research Institute,
Ibaraki 311-01, Japan*

(Received 10 July 1995)

Abstract

Toroidicity-induced Alfvén eigenmodes (TAE modes) are investigated in JT-60U in ITER-relevant conditions, i.e., the plasma current (I_p) up to 4 MA and the safety factor down to 2.8, using second harmonic minority ion ICRF heating. Higher n (toroidal mode number) modes appear with increasing I_p . Reduction of MeV ion population due to TAE modes is in proportion to TAE mode amplitudes, but becomes less important at high density, although TAE amplitudes are still large. It is demonstrated that the non-inductive current profile control method is effective for control of TAE modes.

Keywords:

TAE modes, JT-60U, ITER, second harmonic ICRF heating, minority ion, toroidal mode number, high- n mode, MeV ion, current profile control, non-inductive current drive,

1. Introduction

It was pointed out in theory that the toroidicity of a plasma column induces a gap in the Alfvén continuum spectrum due to the poloidal mode coupling and that the shear Alfvén waves, whose frequency is within the gap, can be unstable in a fusion reactor, since fusion alpha particles can resonate with shear Alfvén waves [1,2]. These modes are called the toroidicity induced Alfvén eigenmodes (TAE modes). If TAE modes become unstable, then fusion alphas undergo enhanced pitch angle scattering and are expelled from the plasma core to the first wall or the periphery region [3], resulting in degradation of plasma performance. Furthermore, if those particles are trapped in the toroidal field ripple, damage of the first wall due to ripple loss particles [4] may be enhanced. Therefore, TAE modes are potentially dangerous for a fusion reactor

and so study of the TAE modes is important for development of a fusion reactor. In experiment, TAE modes were observed for the first time in TFTR [5], and subsequently in DIII-D [6]. In those experiments, tangential neutral beam injection (NBI) was employed. TAE modes became unstable when the fast ion velocity in the parallel direction approached the Alfvén speed. Later on, it was demonstrated in TFTR that TAE modes can be also excited by ICRF minority ion heating through the precessional magnetic drift and bounce resonance [7,8]. Recently, TAE modes were also observed in JET [9] and JT-60U [10] during ICRF heating and/or NBI heating.

In TFTR D-T experiments, TAE modes driven by fusion alpha particles have not yet been observed, although some efforts were devoted to drive TAE modes [11]. The alpha beta values may be still too low

to drive TAE modes [12]. In JET, excitation of TAE mode by external coils was attempted and damping rates were measured for the basic research of TAE modes [13].

The prediction of TAE modes for ITER [14] by global stability codes shows that TAE modes may be a problem at high toroidal mode numbers ($6 < n < 50$) [15]. Therefore experiments in the high n regime are quite important. TAE modes experiments with ICRF heating in JT-60U are characterized by high plasma current and low safety factor, namely I_p up to 4 MA and the effective safety factor at the edge q_{eff} [16] down to 2.8. In these conditions, TAE modes with high toroidal mode number appear (n at least 13) [17]. These results on the excitation of high n TAE modes in JT-60U were reported in previous papers [17,18]. In parallel with the study of characteristics of high n TAE modes, the evaluation of fast ion losses and impact on the plasma confinement due to TAE modes and the control method of TAE modes should be investigated for the development of a fusion reactor.

This paper presents overall results on the JT-60U TAE mode experiments, with detailed description on the excitation of TAE modes including ICRF heating conditions, the impacts on the fast ion and bulk plasma confinement, and control of TAE modes through the current profile control including the lower hybrid current drive. In large tokamaks, the sawtooth stabilization by fast ions [19] is generally observed during ICRF heating and is an important element to affect the plasma confinement in various aspects. This paper also makes clear the relation between the TAE modes and the sawtooth stabilization.

In section 2, outline and features of the JT-60U TAE mode experiments are presented. In section 3, excitation of TAE modes, including resonant energy, threshold tail ion stored energy and ICRF heating conditions, is discussed. In section 4, the impacts of TAE modes, such as fast ion losses and degradation of the bulk plasma energy confinement are discussed. In section 5, the control of TAE modes through the current profile control including effects of the sawtooth relaxation is discussed. A discussion and conclusions are given in section 6.

2. Outline and Features of TAE Mode Experiments on JT-60U

2.1 Experimental Conditions

TAE modes are observed in JT-60U both in ICRF heated discharges and quasi-perpendicular NBI heated discharges. For ICRF heating, the second harmonic hydrogen minority heating of deuterium or helium (^4He) plasmas is employed. The operating frequency is set to be 116 MHz, which corresponds to the second harmonic cyclotron resonance frequency of hydrogen at 3.8 T. Two sets of 2×2 loop antenna array [20,21], located on the low field side midplane, are employed. Figure 1 shows the cross-section of the JT-60U vacuum vessel and the ICRF antenna, including a typical plasma equilibrium for ICRF experiments. TAE modes are excited by the ICRF heating over wide ranges of the plasma current, the safety factor and the electron density, i.e., the plasma current $I_p = 1.5 - 4$ MA, the safety factor $q_{\text{eff}} = 7.2 - 2.8$ and the line average electron density $\bar{n} = (1.1 - 4.5) \times 10^{19} \text{ m}^{-3}$ with $B_T \sim 3.8$ T. Thus the ICRF heating is a useful means for TAE mode study in JT-60U. On the other hand, for excitation of TAE modes with perpendicular NBI heating (80 keV deuterium beam), the toroidal field was limited at around 0.6T.

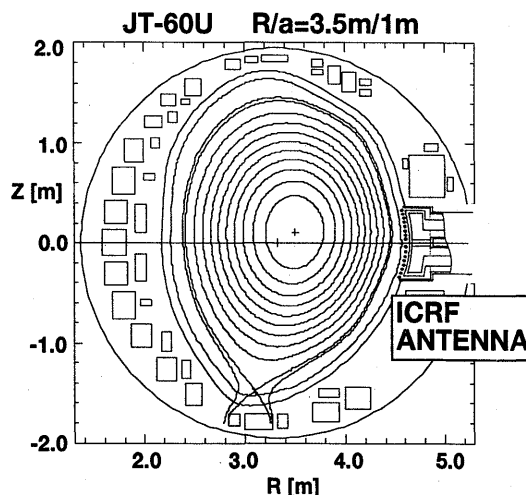


Fig. 1 Cross-section of the JT-60U vacuum vessel and the ICRF antenna, including a typical plasma equilibrium for ICRF heating.

2.2 Identification of TAE Modes

TAE modes were identified by checking the mode frequencies measured by magnetic probes (Mirnov coils) installed inside the vacuum vessel. Mirnov coil signals are digitized at 200 kHz for fast Fourier-transform (FFT) analysis. For frequencies above 100 kHz, however, the measured frequency (f (kHz)) can be corrected to be $200 \pm f$ kHz by the side band effect. The upper limit is determined by the cut-off frequency of the probe system (~ 300 kHz). We calibrated thus obtained FFT data by a spectrum analyzer. As a result, the real mode frequencies were found to be exactly given by $200 \pm f$ kHz for a practical range of TAE experiments by ICRF heating on JT-60U. The calibrated frequencies (f_{ex}) are plotted as a function of \bar{n}_e in Fig. 2, where $I_p=3$ MA ($q_{eff} \sim 3.6$). Full (open) circles designate the upper (lower) boundary of the mode frequencies because multi-mode peaks appear in the frequency spectrum [17]. The calibrated frequencies are well fitted by the electron density dependence of theoretical TAE frequency ($f_{TAE} = v_A/(4\pi qR) \propto \bar{n}_e^{-0.5}$) [1], where $v_A (=2.18 \times 10^{16} B/(An_i)^{0.5}$ [m/s]) is the Alfvén speed, B the total magnetic field, A the mass number, n_i the ion density, q the local safety factor and R the major radius. The value of q is chosen to be 1.24. From this good agreement with the theoretical dependence of the TAE mode frequency on the electron density with reasonable q -value (justified in Ref.

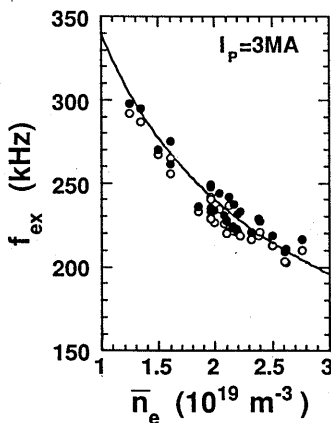


Fig. 2 Measured mode frequencies as a function of the line-average electron density. Full (open) circles designate upper (lower) boundary of the multi-mode peaks. The solid curve indicates the theoretical TAE mode frequency with $q=1.24$ and $B=3.8$ T.

[18]), we conclude that these modes are TAE modes. Mirnov coil signals of the poloidal array show that TAE mode amplitudes are strongly localized on the low field side, as observed in DIII-D [6].

2.3 Identification of Toroidal Mode Numbers

We identified the toroidal mode number, using Doppler shift effect due to the toroidal plasma rotation. The toroidal rotation velocity is controlled by adjusting tangential neutral beam power. Typical example is shown in Fig. 3. ICRF power is injected from 6.5 sec to 9 sec. Tangential neutral beam power is varied from a counter-direction to a co-direction. TAE modes appear shortly after ICRF turn-on. Time evolution of their amplitudes is shown in the top two columns in Fig. 3, discriminated odd and even modes. The toroidal rotation velocity at $r=0.36$ m, which is within the estimated location of the amplitude peak of

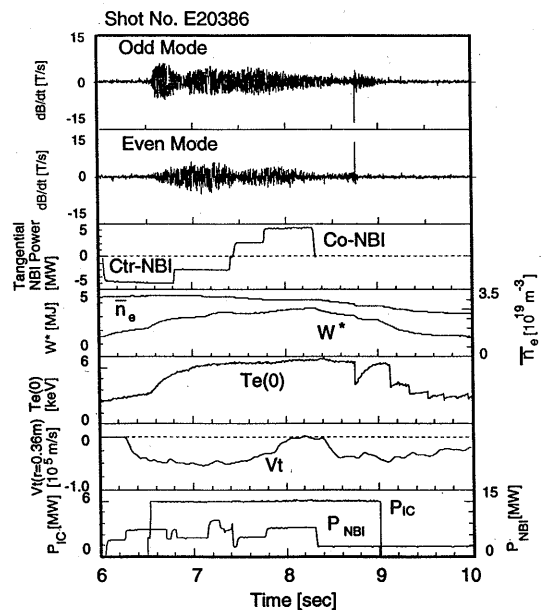


Fig. 3 Typical example of controlling the toroidal rotation velocity during ICRF heating for the purpose of identification of toroidal mode numbers, showing the Mirnov coil signals of an odd and an even toroidal mode, the tangential NBI power, the line average electron density, the diamagnetic stored energy, the central electron temperature, the toroidal rotation velocity at $r=0.36$ m measured from the charge exchange recombination spectroscopy at the C VI transition, the ICRF power and the NBI power. $I_p=3$ MA and $B_T(0)=3.7$ T.

TAE modes, changes from negative value to approximately zero by changing from counter-beam to co-beam. At the period of almost zero toroidal rotation velocity, the electron density is almost constant. The sawtooth oscillation is stabilized up to 8.75 sec.

Time evolution of the frequency spectra of TAE

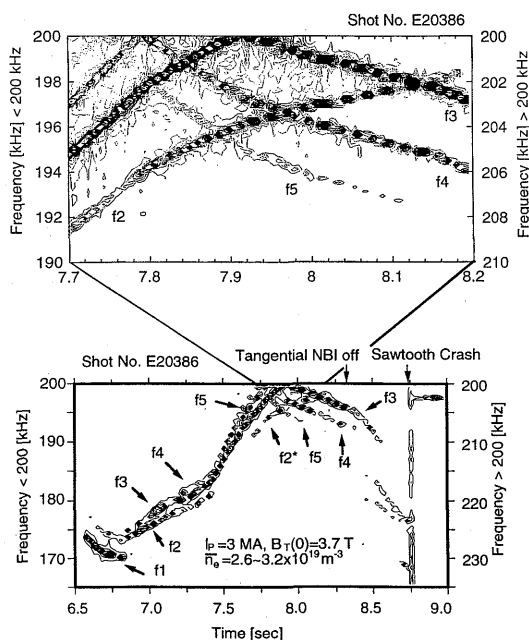


Fig. 4 Time evolution of the frequency spectra of TAE modes during the toroidal rotation velocity scan shown in Fig 3.

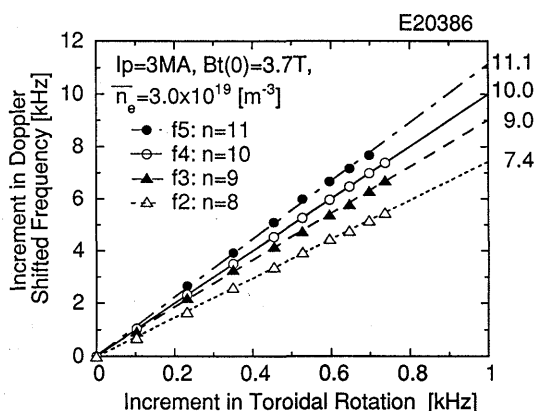


Fig. 5 The time increment of the TAE mode frequency due to Doppler shift against the increment in the toroidal rotation frequency.

modes during scanning toroidal rotation in Fig. 3 is shown in Fig. 4. The bottom figure corresponds to the full ICRF pulse. Five discrete modes are seen in this case. Note that the frequency spectra measured by magnetic probes are displayed using the side band effect of 200 kHz sampling as mentioned in Sec. 2.1. The left vertical axis is for signals below 200 kHz, while the right vertical axis is for signals over 200 kHz. The mode frequency change is caused by the Doppler shift due to the toroidal rotation and also a change of the density. The top figure is an extended view for the period when the electron density is almost constant. The frequency change here is mainly due to the change of the toroidal rotation velocity. Frequency intervals between each mode are different, suggesting that these modes have different toroidal mode numbers.

In Fig. 5, time increments of the TAE mode frequencies are plotted against increments in the toroidal rotation frequency. Here we take the increment in the toroidal rotation frequency to be one tenth of the change of the TAE mode frequency of $n=10$ mode. Then frequencies of adjacent modes (f_5 and f_3) are on lines of $n=11$ and $n=9$. For f_2 , the frequencies shifts are on the line of somewhat lower value than that of $n=8$, but it is reasonable because the lower frequency mode is located on larger radius and feels slower toroidal rotation speed there. Thus, it is confirmed that the toroidal mode number increases one by one during sawtooth free period by scanning the toroidal rotation velocity with tangential NBI. In this example, as shown in Fig. 4, the toroidal mode number starts with an odd number of 7 and gradually increases to 11. The situation is consistent with the time evolution of odd and even modes in the early stage, as indicated in Fig. 3. The first mode is odd, the second one is even and the third one is odd.

Alternatively, the toroidal mode number can be derived from the frequency shift between neighbouring two modes. The Doppler-shifted (measured) TAE mode frequencies for neighbouring two modes are written as

$$f_{DS}^{(n)} = f_{TAE}^{(n)} + n\Phi_t^{(n)} \quad (1)$$

$$f_{DS}^{(n+1)} = f_{TAE}^{(n+1)} + (n+1)\Phi_t^{(n+1)}, \quad (2)$$

where $f_{DS}^{(n)}$ and $f_{TAE}^{(n)}$ are the Doppler-shifted and TAE-mode frequencies of the n -th mode, respectively, and $\Phi_t^{(n)}$ is the toroidal rotation frequency where the

n -th mode exists. $f_{\text{TAE}}^{(n)}$ is expressed as [1]

$$f_{\text{TAE}}^{(n)} = v_A / (4\pi q R), \quad (3)$$

where

$$q = (2m + 1) / 2n, \quad (4)$$

and m is the poloidal mode number. Letting the frequency shift between the two mode $\Delta f_{\text{DS}}^{(n)} = f_{\text{DS}}^{(n+1)} - f_{\text{DS}}^{(n)}$, and $\Phi_t^{(n)} = \Phi_t^{(n+1)} = \Phi_t$, then the toroidal mode number is given by

$$n \cong \sqrt{\frac{f_{\text{TAE}}|_{q=1}}{2(\Delta f_{\text{DS}}^{(n)} - \Phi_t)}} - 1 \quad \text{for } m = n \quad (5)$$

and

$$n \cong \sqrt{\frac{3f_{\text{TAE}}|_{q=1}}{2(\Delta f_{\text{DS}}^{(n)} - \Phi_t)}} - 2 \quad \text{for } m = n + 1, \quad (6)$$

where $f_{\text{TAE}}|_{q=1} = v_A / (4\pi R)$. At 8 sec (the stationary phase) in Fig. 3, the frequency shift between neighbouring two modes, $\Delta f_{\text{DS}}^{(i)}$ ($i=2-4$) are 3.9 kHz, 3.0 kHz and 2.4 kHz, respectively, from Fig. 4. In the present case, $m=n+1$ holds [17]. Then, we have $n=7.7$ for f2, $n=9.0$ for f3 and $n=10.3$ for f4. These are similar to those obtained from the change of the toroidal rotation frequency. Note that the frequency shift method was applied here for the stationary phase. Thus the two methods give similar answer from the different approaches, indicating reliability of the estimation of the toroidal mode number. Practically, the frequency shift method may be useful to know an upper limit of the toroidal mode number without the data of the toroidal rotation frequency in the near uniform rotation profile case (i.e., $\Phi_t^{(n)} \sim \Phi_t^{(n+1)} < 0$). The minus sign of the rotation frequency during ICRF heating was confirmed in JT-60U, similarly as in other tokamaks [22]. Φ_t is in the order of -1 kHz in JT-60U.

2.4 High n TAE Modes

Figure 6 shows the number of TAE modes appearing during an ICRF heating pulse as a function of the plasma current. The number of TAE modes increases with increasing plasma current. As many as nine TAE modes were observed at $I_p=4$ MA. On the other hand, the local safety factor of TAE modes,

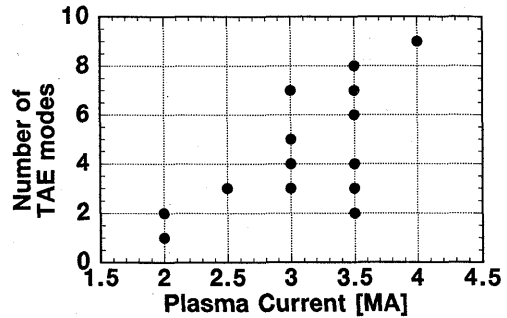


Fig. 6 The number of TAE modes appearing during an ICRF heating pulse as a function of the plasma current.

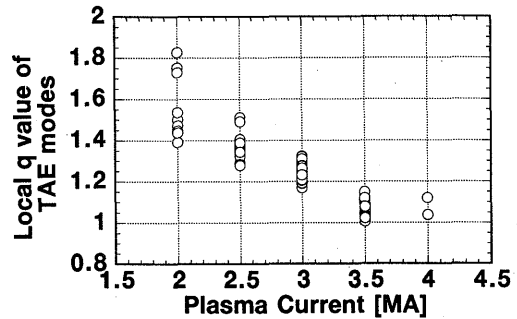


Fig. 7 The local safety factor of TAE modes, which is evaluated from $q = v_A / 4\pi R f_{\text{ex}}$, as a function of the plasma current.

which is evaluated from $q = v_A / 4\pi R f_{\text{ex}}$, is plotted as a function of the plasma current in Fig. 7. The local safety factor is approaching to unity with increasing I_p . These results suggest that higher n mode tends to appear in high I_p regime, since q is expressed as $q = (2m+1)/2n$, and $q \approx 1$ is satisfied for $m \sim n \gg 1$.

Time evolution of the frequency spectra of TAE modes of a 4 MA discharge is shown in Fig. 8. Nine TAE modes appear during a sawtooth-free period, where individual modes appear and disappear one after another in relatively narrow frequency band. Those frequencies change due to the Doppler shift by the toroidal rotation because the electron density is almost constant during this period. The phenomena can be understood by the Alfvén continuum gap map shown in Fig. 9. The ordinate is the safety factor q where the TAE gaps are located, which is given by $q = (2m+1)/2n$, and the abscissa is the toroidal mode number. Each dot shows the Alfvén continuum gap of

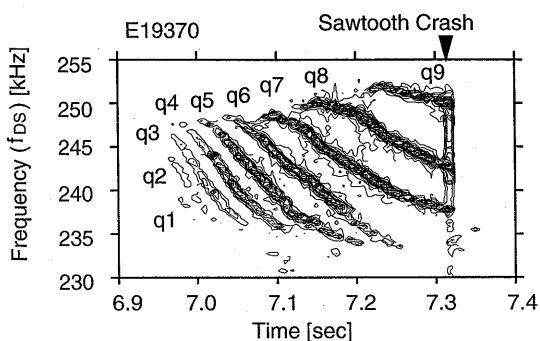


Fig. 8 Time evolution of the frequency spectra of TAE modes of a 4 MA discharge.

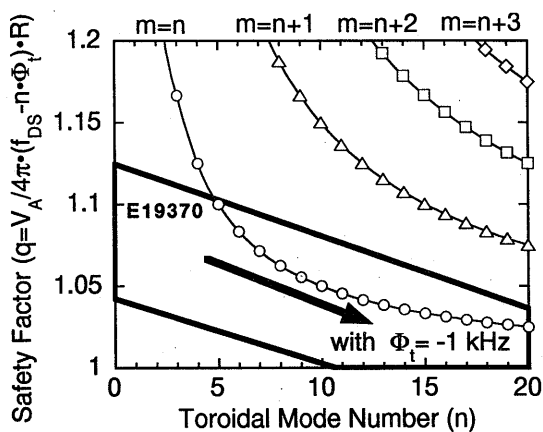


Fig. 9 The Alfvén continuum gap map.

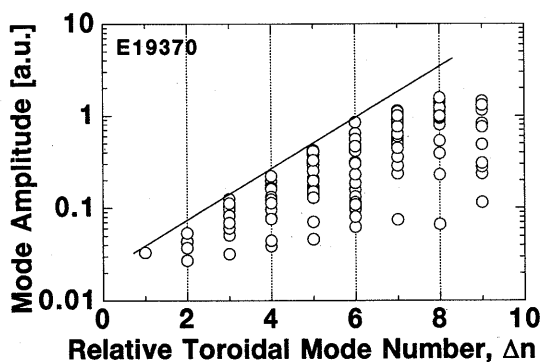


Fig. 10 Peak amplitudes of the frequency spectra shown in Fig. 8, as a function of the relative toroidal mode number Δn .

TAE modes. Curves are $m-n = \text{constant}$ lines. We identified that, in 3 MA discharge, TAE modes appear along the line of $m=n+1$ [17]. For I_p of 3.5–4 MA, the range of the local safety factor is 1.0 ~ 1.18 as indicated in Fig. 7. Then we can infer that TAE modes appear along the line of $m=n$ for I_p of 3.5–4 MA. The domain surrounded by bold full lines is determined assuming the toroidal rotation frequency of $\Phi_t = -1$ kHz. Here, q is given by $q = v_A / (4\pi R (f_{DS} - n\Phi_t))$ including the plasma toroidal rotation. During a sawtooth-free period, the q -profile becomes peaked and the local safety factor gradually decreases [23]. Therefore, from this mapping, we can infer that the toroidal mode number increases one by one along the $m=n$ line during a sawtooth-free period. A possible range of the toroidal mode numbers which appeared sequentially in the 4 MA discharge is, for example, given by $n = \Delta n + (4 \sim 5)$, $\Delta n = 1 \sim 9$. Note that the lower boundary of the range may be a minimum estimate. So, the highest toroidal mode number can be estimated to be at least 13.

Figure 10 shows peak amplitudes of the frequency spectra shown in Fig. 8, as a function of the relative toroidal mode number Δn . The maximum values of TAE mode amplitudes increase exponentially with increasing n up to about 10 and then tend to saturate against n up to at least $n=13$. Such a behaviour cannot be explained by local TAE stability theories [18]. Analysis with a global stability code (NOVA-K [24]) is in progress [25]. A nonlinear theory [26,27] is also needed for analyzing such a behaviour.

3. Excitation of TAE Modes

3.1 Resonant Energy of Trapped Ions

ICRF heating produces energetic trapped ions. The wave-particle resonance for excitation of TAE modes by trapped ions [28] can be written as

$$\omega_{\text{TAE}} - n \langle \omega_d \rangle - p \omega_b = 0, \quad (7)$$

where ω_{TAE} is the TAE mode frequency ($= 2\pi f_{\text{TAE}}$), $\langle \omega_d \rangle$ the bounce-averaged precessional drift frequency, ω_b the bounce frequency and p an integer. For deeply trapped ions, $\langle \omega_d \rangle$ and ω_b are given by $\langle \omega_d \rangle = q E_i / (m_i r R \omega_c)$ and $\omega_b = \varepsilon^{1/2} v / (qR)$, respectively, where E_i is the ion energy, m_i the ion mass, r the minor radius, ω_c the ion cyclotron frequency, $\varepsilon = r/R$ and v the ion speed. From eq. (7), the resonant energy decreases with increasing n . For low- and medium- n , the bounce

resonance is important. For high- n TAE modes, the precessional magnetic drift resonance is dominant [29]. The resonant ion energy for the precessional magnetic drift resonance is expressed as

$$E_{\text{res}} \approx ZeBrv_A / (2nq^2), \quad (8)$$

where Z is the ion charge number. For typical experimental parameters ($Z=1$, $B_T=3.8$ T, $r=0.5$ m, $v_A=1.2 \times 10^7$ m/s, $q=1.1$), we have $E_{\text{res}} \approx 9.4/n$ (MeV). Thus MeV trapped ions should play a dominant role in excitation of TAE modes. Actually we observed correlation of MeV protons with TAE modes during ICRF heating (see Sec. 4.1). A ratio of the resonant ion speed to the Alfvén speed is written as

$$\frac{v_{\text{res}}}{v_A} \approx \frac{6.8 \times 10^{-9}}{q} \sqrt{\frac{Zer(An_i)^{0.5}}{m_i n}}. \quad (9)$$

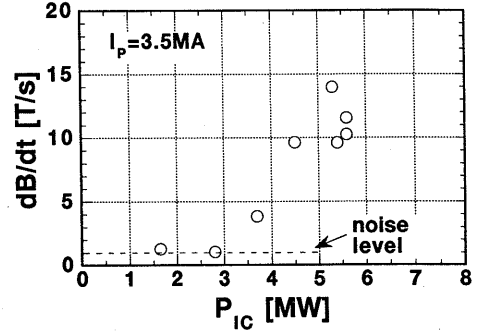
For the typical parameters mentioned above, $v_{\text{res}}/v_A \approx 3.5/n^{0.5}$. The resonant ion speed is in the order of the Alfvén speed, similarly to the resonant condition by passing particles. In the case of passing particles, the resonant condition is given by $v_{\text{res}}/v_A \geq 1$ (or $v_{\text{res}}/v_A \geq 1/3$ including the side band effect) in theory [28], while $v_f/v_A \approx 1$, where v_f is an injected fast ion speed, was observed for the excitation condition of TAE modes in DIII-D experiments using tangential NBI [30].

3.2 Threshold Tail Ion Stored Energy

The threshold tail ion stored energy was explored by scanning ICRF power in a narrow range of the line average electron density. Figure 11 (a) shows TAE mode amplitudes measured by the Mirnov coil as a function of the ICRF power, P_{IC} at $\bar{n}_e = 2.1 - 2.6 \times 10^{19} \text{ m}^{-3}$. The TAE mode amplitude increases nonlinearly with P_{IC} and the threshold heating power is about 3.5 MW. The corresponding tail ion stored energy (W_{tail}) is evaluated to be $W_{\text{tail}} = 2/3 (W_{\text{dia}} - W_{\text{th}})$, where W_{dia} and W_{th} are diamagnetic and kinetic plasma stored energies, respectively. Figure 11 (b) shows W_{tail} versus P_{IC} . W_{tail} increases somewhat nonlinearly with P_{IC} . The fast ion stored energy threshold is about 0.3 MJ, and the beta threshold of tail ions, $\langle \beta_{\text{tail}} \rangle$, is 0.05%.

The experimental result is compared with calculation by the global stability code (NOVA-K) [10]. The calculation was made employing the plasma equilibrium and plasma parameters of a typical TAE mode

a)



b)

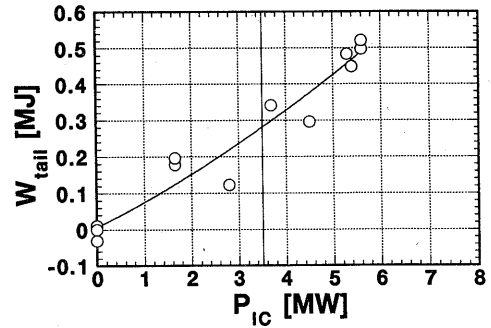


Fig. 11 (a) TAE mode amplitudes measured by the Mirnov coil as a function of ICRF heating power for $\bar{n}_e = (2.1 - 2.6) \times 10^{19} \text{ m}^{-3}$. (b) Corresponding tail ion stored energy as a function of ICRF heating power.

shot (E19332, shown in Fig. 14). The threshold beta value of fast ions was calculated as a function of the fast ion pressure scale length (L_h) normalized by the minor radius for $n=4$ and $n=7$ modes. Two TAE modes appear for each toroidal mode number, whose frequencies are almost consistent with those of experiment. The threshold fast ion beta value, which is insensitive to L_h in the range of $L_h/a = 0.3 - 0.5$, is in the order of 0.01%, which is consistent with the experimental value mentioned above.

3.3 ICRF Heating Conditions

3.3.1 Resonance position

As to the ICRF heating conditions for excitation of TAE modes, we first investigate effects of the ion cyclotron resonance layer position on the excitation of TAE modes, which is also important for the sawtooth stabilization [31]. Figure 12 shows the results on the resonance position scan by changing the toroidal field in 3 MA discharges. A deviation of the resonance position from the plasma center normalized by the

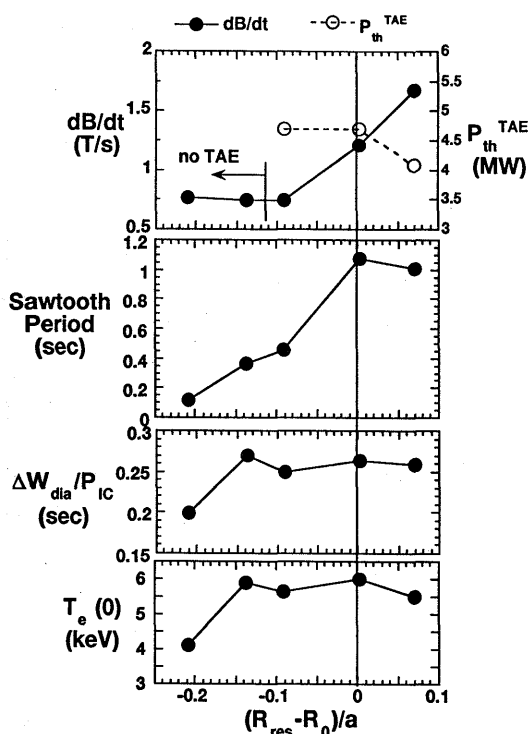


Fig. 12 Results of the ICRF resonance position scan experiment, showing the TAE mode amplitude (Mirnov coil signals), the threshold ICRF power, the sawtooth-free period, the heating rate and the central electron temperature, as a function of $(R_{res} - R_0)/a$.

minor radius, $(R_{res} - R_0)/a$, changes from -0.2 to 0.07 . TAE modes were observed for $|R_{res} - R_0|/a < 0.1$. It is also indicated in the figure that excitation of TAE modes is relatively easy for low field side resonance position with respect to the magnetic axis. Such an asymmetry around the on-axis resonance is also found in the sawtooth stabilization. Sawtooth-free periods were greatly extended for $(R_{res} - R_0)/a > 0$. The result suggests that deeply trapped ions, which tend to be produced for low field side resonance with respect to the magnetic axis, plays an important role in excitation of TAE modes as well as the sawtooth stabilization.

The heating rate, $\Delta W_{dia}/P_{IC}$, where ΔW_{dia} is an incremental diamagnetic stored energy by the ICRF heating power, and the central electron temperature are almost constant for $-0.14 \leq (R_{res} - R_0)/a \leq 0.07$ as indicated in Fig. 12. The results suggests that slightly off-axis resonance to the high field side may be effective for efficient core heating, avoiding TAE modes.

3.3.2 Electron density and minority concentration ratio

It is found that the electron density and the minority proton concentration ratio are important parameters for excitation of TAE modes and the sawtooth stabilization as well as the heating rate. Figure 13 shows a parameter domain where TAE modes were observed (TAE domain) with on-axis resonance in 3 MA discharges. Lower proton concentration ratio and lower electron density tend to make excitation of TAE modes more difficult. A domain where sawtooth-free periods are longer than 0.6 sec ($\sim 2 \times \tau_E$) is also indicated, in Fig. 13. We call this an SST domain. The two domains almost coincide, although the TAE domain expands to somewhat lower density range than the SST domain. The heating rate is better ($\Delta W_{dia}/P_{IC} > 0.2$ sec) only within the TAE/SST domains. In other words, TAE modes are excited only when the heating is successful, although TAE modes degrade the core plasma energy confinement through the loss of energetic ions to some extent (see Sec. 4.2 and Sec. 4.3). A possible reason why the heating is poor in low density or small proton concentration may be that the ICRF heating power deposition profile becomes so

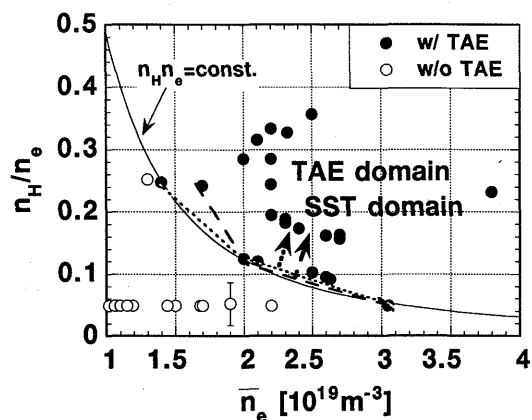


Fig. 13 Parameter domain where TAE modes were observed (TAE domain, delimited by the dotted line). The ordinate is the proton to electron density ratio. Full circles designate a shot where TAE modes appeared, while open circles designate a shot where TAE modes did not appear. The parameter domain for the sawtooth stabilization (SST domain, delimited by the broken line, is also indicated. The thin solid line indicates that $n_H n_e = \text{const.}$ ICRF on-axis heating in 3 MA discharges. $P_{IC} = (4.2 - 7)$ MW.

broad because of the orbit effect of fast ions. The orbit effect may set in above some critical energy of fast ions. The temperature of the fast ions T_H scales as $T_H \propto P_{IC} T_e^{1.5} / (n_H n_e)$. For given P_{IC} and T_e , $T_H \propto 1 / (n_H n_e)$. The thin solid curve in Fig. 13 indicates a $n_H n_e = \text{constant}$ line which lies closely along the TAE/SST domains. This supports the hypothesis that the heating is limited by the orbit effect of fast ions. Above some critical energy, fast trapped ions can always feel the RF electric field because of the Doppler broadening of the resonance layer. Orbits of such particles become larger and larger, and may be quickly lost to the first wall.

4. Impact of TAE modes

4.1 Typical Example

Time evolution of a typical shot where TAE modes were prominently excited is shown in Fig. 14, which clearly indicates impact of TAE modes on the

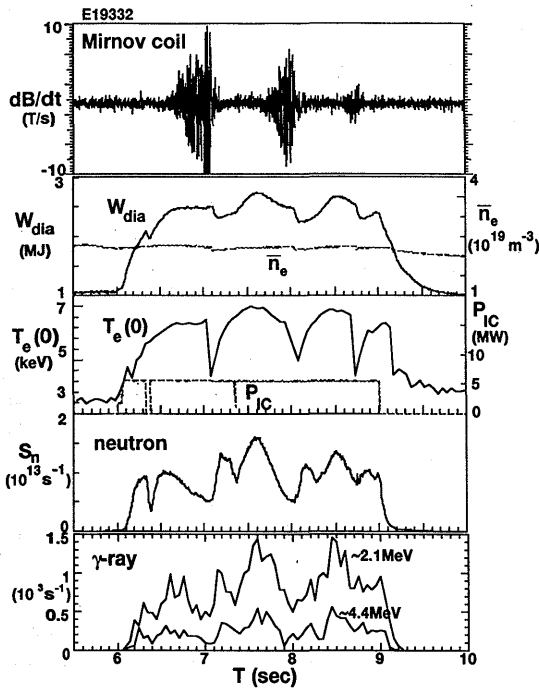


Fig. 14 Time evolution of a typical shot where TAE modes appeared, showing the Mirnov coil signal (dB/dt), the diamagnetic stored energy, the line average electron density, the central electron temperature, the ICRF power, the neutron rate and the γ -ray signals (~ 2.1 MeV and ~ 4.4 MeV). ${}^4\text{He} + (\text{H})$ discharge, $I_p = 3.5$ MA, $q_{\text{eff}} = 3.2$, $\bar{n}_e = 2.2 \times 10^{19} \text{ m}^{-3}$ and $P_{IC} = 5.3$ MW.

fast ion confinement and the bulk plasma confinement. The experiment was done with a ${}^4\text{He} + (\text{H})$ discharge, where a species within parentheses is a minority ion component. By the TAE modes, the plasma stored energy and the central electron temperature were saturated during the first sawtooth stable period or decreased during the second- and third-stable period. Reduction of the total stored energy $W_{\text{tot}} (= W_{\text{th}} + W_{\text{tail}}$; W_{th} is the thermal plasma stored energy and W_{tail} is the tail ion stored energy) due to the TAE modes is $\sim 7\%$, which is similar to the reduction due to the subsequent giant sawtooth crash. However, a fraction of the loss of the tail component to the total loss ($\Delta W_{\text{tail}} / \Delta W_{\text{tot}}$) due to the TAE modes is $\sim 70\%$, which is higher than that by the sawtooth crash ($\sim 40\%$). Specifically, effects of TAE modes on MeV protons are prominent. The neutron yield shown in Fig. 14 is originated mainly from the boron-proton nuclear reaction (${}^{11}\text{B}(p,n){}^{11}\text{C}$) [18]. It reflects protons whose energy is more than 3 MeV. The 2.1 MeV and 4.4 MeV γ -rays come from inelastic scattering of fast protons with borons and carbons and reflects protons whose energy is more than 2.5 MeV and 5 MeV, respectively. MeV protons decrease by 60–70% due to TAE modes, although the reduction rate in the stored tail ion energy ($\Delta W_{\text{tail}} / W_{\text{tail}}$) is only 20%. Thus the TAE modes affect the population of MeV protons dominantly.

4.2 Fast Ion Loss

We investigate loss of MeV ions due to TAE modes by scanning \bar{n}_e from $1.5 \times 10^{19} \text{ m}^{-3}$ to $4.5 \times 10^{19} \text{ m}^{-3}$ at the plasma current of 3.5 MA and the toroidal field of 3.8 T with a fixed range of the ICRF power of 5–5.5 MW. The internal inductance stays in a narrow range ($l_i = 1.15$ – 1.2) against the change of \bar{n}_e . Figure 15 shows amplitudes of TAE modes measured by the Mirnov coil as a function of \bar{n}_e . Here, the ordinate (TAE mode amplitude) is the Mirnov coil signal (dB/dt) multiplied by $(\bar{n}_e)^{0.5}$ in order to compensate change of TAE mode frequency due to the change of \bar{n}_e . In the low density region ($\bar{n}_e = 1.5$ – $2.5 \times 10^{19} \text{ m}^{-3}$), the TAE mode amplitude increases with \bar{n}_e and tends to be constant above $\bar{n}_e \sim 2.5 \times 10^{19} \text{ m}^{-3}$. This behaviour clearly indicates existence of a lower limit of the electron density for excitation of TAE modes, which is below $1.5 \times 10^{19} \text{ m}^{-3}$, with fixed ICRF power. Corresponding tail ion stored energy, which is evaluated from the diamagnetic data and the kinetic data (see

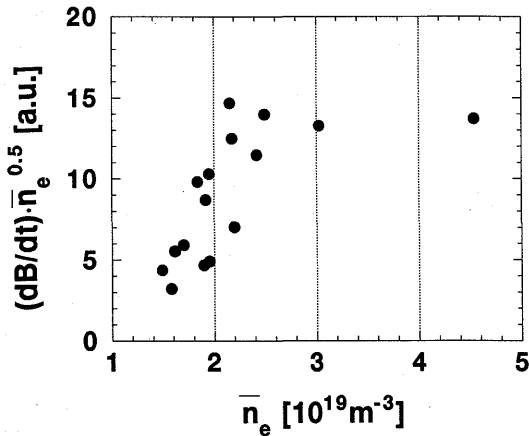


Fig. 15 Normalized TAE mode amplitudes measured by the Mirnov coil as a function of the line average electron density. ⁴He + (H) discharges, $I_p=3.5$ MA, $q_{\text{eff}}=3.2$, and $P_{\text{IC}}=(5-5.5)$ MW.

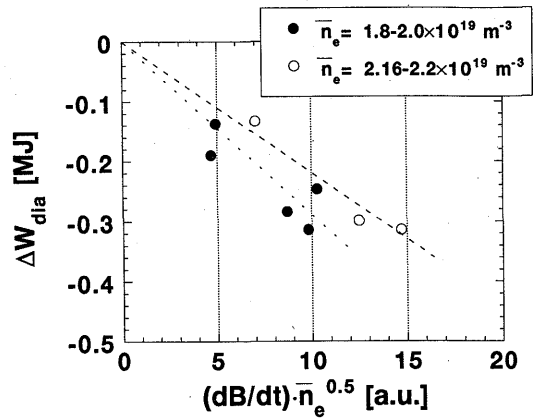


Fig. 17 The decrease in diamagnetic stored energies due to TAE modes as a function of the normalized TAE mode amplitudes.

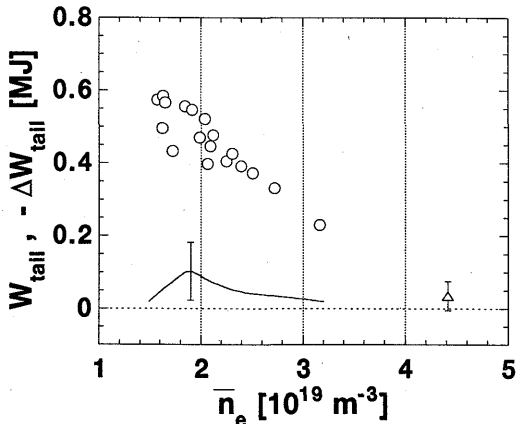


Fig. 16 Tail ion stored energy just before onset of TAE modes in sawtooth-free period (open circles) and with TAE modes and sawtooth oscillation (an open triangle) as a function of the line average electron density in the same experimental run as in Fig. 15. The solid line indicates the decrease in tail ion stored energies due to TAE modes.

Sec. 3.2), as a function of \bar{n}_e is shown in Fig. 16. Open circles are tail ion stored energy just before onset of TAE modes during a sawtooth stable period, while an open triangle is the one with TAE modes and sawtooth oscillation. At such a high density, the sawtooth could not be stabilized. The tail ion stored energy thus greatly decreases with increasing electron density, although it is confirmed that these data are roughly in

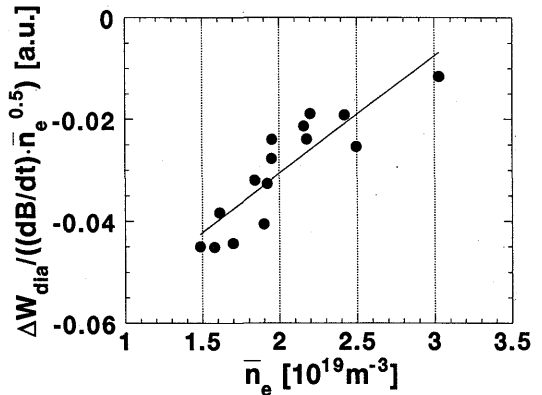


Fig. 18 The decrease in diamagnetic stored energies due to TAE modes divided by the normalized TAE mode amplitude, as a function of the line average electron density.

proportion to the classical slowing-down time. It is interesting that TAE modes are still strongly excited in the high density plasma where the tail ion beta value is at most only about 0.01%. It suggests that the damping terms for TAE modes also more rapidly decrease with increasing electron density. Detailed study on this behaviour, however, is beyond the scope of this paper. Figure 16 also shows the decrease in tail ion stored energies due to TAE modes. It appears that the loss of the tail ion stored energy has a broad peak at \bar{n}_e around $2 \times 10^{19} \text{ m}^{-3}$ and becomes smaller with increasing density, where the TAE mode amplitudes are almost constant. For further discussion on the impact of

TAE modes, we employ ΔW_{dia} , a change of the diamagnetic stored energy due to TAE modes, because of a large error bar for ΔW_{tail} .

Figure 17 shows ΔW_{dia} as a function of TAE amplitudes corrected by the electron density. Solid circles are for $\bar{n}_e = (1.8-2.0) \times 10^{19} \text{ m}^{-3}$, while open circles are for $\bar{n}_e = (2.16-2.2) \times 10^{19} \text{ m}^{-3}$. If the density range is wide, the data are scattered and there seems no correlation between them. But, if the density range is limited like in Fig. 17, the correlation between them is clearly seen. The diamagnetic stored energy decreases as TAE mode amplitudes increase.

Then, ΔW_{dia} divided by the TAE mode amplitude is a more general quantity. Figure 18 indicates that ΔW_{dia} per unit TAE amplitudes becomes smaller with increasing electron density, which means that the impact of TAE modes becomes smaller with increasing density. The loss of the plasma stored energy by TAE modes is dominated by fast ions as discussed above. Therefore, the result indicates that the loss of energetic ions becomes smaller with increasing electron density although TAE amplitudes are still large.

Above results on the loss of tail ion stored energy by the diamagnetic measurements are further validated by the neutron and γ -ray data. Here, the neutron data, which reflect protons whose energy is higher than 3 MeV through the $^{11}\text{B}(p, n)^{11}\text{C}$ reaction, are employed because of its better statistics than those of the γ -ray data.

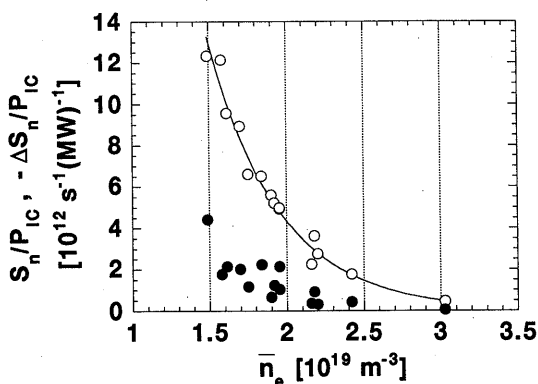


Fig. 19 The neutron count just before onset of TAE modes (open circles) and the decrease in neutron counts due to TAE modes (full circles) as a function of the line average electron density in the same experimental run as in Fig. 15. The data are normalized by ICRF power.

Figure 19 shows the neutron yield in the same experimental run as in Figs. 15–18. Open circles designate neutron counts, S_n , just before a TAE mode onset, while closed ones designate decreases in neutron counts, ΔS_n , due to TAE modes. Both data are normalized by the ICRF power. S_n decreases exponentially with increasing density. ΔS_n is roughly constant for \bar{n}_e up to $2 \times 10^{19} \text{ m}^{-3}$ except the data point at $\bar{n}_e \sim 1.5 \times 10^{19} \text{ m}^{-3}$ and then steeply decreases. It becomes negligibly small at $\bar{n}_e \sim 3 \times 10^{19} \text{ m}^{-3}$. Note that the scatter of ΔS_n is mainly due to the variation of

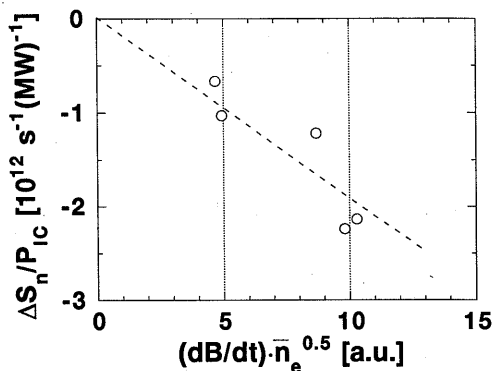


Fig. 20 The decrease in neutron counts due to TAE modes, normalized by ICRF power, as a function of the normalized TAE mode amplitudes for $\bar{n}_e = (1.8-2.0) \times 10^{19} \text{ m}^{-3}$.

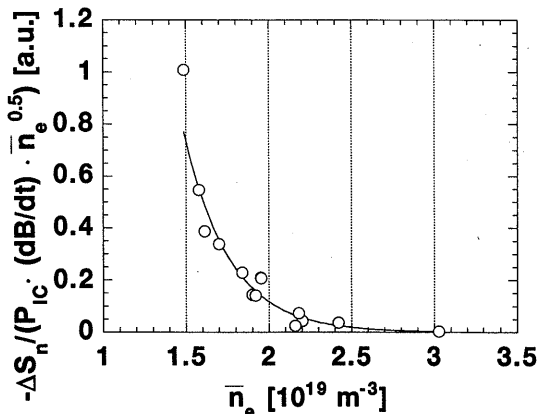


Fig. 21 The decrease in neutron counts due to TAE modes, normalized by ICRF power, divided by the normalized TAE mode amplitude as a function of the line average electron density.

the TAE mode amplitudes at given electron density, as shown in Fig. 15. ΔS_n is plotted as a function of the TAE mode amplitudes for limited range of \bar{n}_e ($1.8-2.0 \times 10^{19} \text{ m}^{-3}$) in Fig. 20. Good correlation is seen between ΔS_n and TAE modes amplitudes similarly as in Fig. 17, where correlation between ΔW_{dia} and TAE modes amplitudes is shown. Then, similarly as in Fig. 18, ΔS_n per unit TAE mode amplitude is plotted as a function of \bar{n}_e in Fig. 21. It is shown that the neutron counts per unit TAE mode amplitude decreases exponentially with increasing electron density and becomes negligibly small at $\bar{n}_e \sim 3 \times 10^{19} \text{ m}^{-3}$.

The reason may be explained as follows; The resonant energy of fast ions scales as $E_{\text{res}} \propto \bar{n}_e^{-0.5} n^{-1}$ from eq. (8), while the average tail temperature scales as $T_{\text{tail}} \propto \bar{n}_e^{-1}$. The resonant ion population scales as $f_{\text{res}} \propto \exp(-E_{\text{res}}/T_{\text{tail}})$ with $E_{\text{res}}/T_{\text{tail}} \propto \bar{n}_e^{0.5} n^{-1}$. Therefore if $n \propto \bar{n}_e^{0.5}$ is satisfied, the resonant ion population is constant against the change of \bar{n}_e . We can roughly estimate the toroidal mode number n with eq. (5) or (6). We obtain $\bar{n} \leq 6$ for $\bar{n}_e \sim 2 \times 10^{19} \text{ m}^{-3}$, whereas $\bar{n} \leq 11$ for $\bar{n}_e \sim 4.5 \times 10^{19} \text{ m}^{-3}$. The result is consistent with the above hypothesis. The observed \bar{n}_e dependence of TAE mode amplitudes in Fig. 15 also suggests this tendency. If the hypothesis is correct, we have $E_{\text{res}} \propto \bar{n}_e^{-1}$. Therefore, the resonant ion energy significantly decreases with increasing \bar{n}_e and the resonant ions become less sensitive for the orbit loss. This may be the reason why the reduction of the stored energy and the neutron counts per unit TAE mode amplitudes greatly decrease with increasing \bar{n}_e .

4.3 Bulk Plasma Energy Confinement

The impact of TAE modes on the bulk plasma is seen in the decrease of the central electron temperature as shown in Fig. 14. The corresponding electron temperature profiles during sawtooth free period with and without TAE modes including just after the giant sawtooth crash are shown in Fig. 22. It is found that TAE modes affect the electron temperature only in the plasma core (well inside the $q=1$ surface). The reason may be explained by reduction of the central heating power due to expelling the fast protons from the core to the outer region by the TAE modes.

Figure 23 shows the central electron temperature as a function of the total heating power, P_{tot} , including the ohmic heating power. The closed circles designate the case with TAE modes, while the open circles indi-

cate the case where the TAE modes are suppressed just after the giant sawtooth crash. The reduction of the central electron temperature due to TAE modes is still moderate, i.e., less than 1 keV. Note that some saturation of the electron temperature is found for P_{tot} above $\sim 7 \text{ MW}$ even without TAE modes, possibly because of the orbit effect.

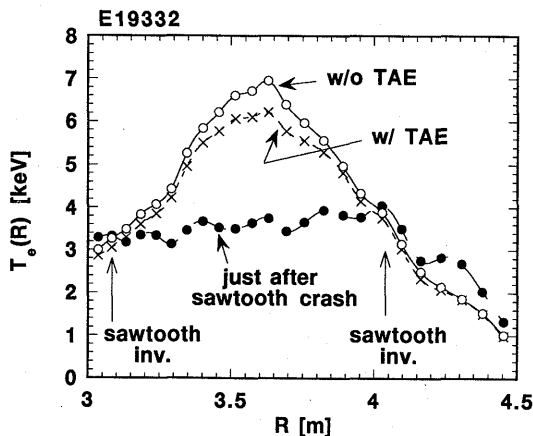


Fig. 22 Electron temperature profiles of the shot in Fig. 14, measured from the Fourier spectroscopy of the electron cyclotron emission. Profiles during sawtooth free period with and without TAE modes at 7.0 sec and 7.6 sec, respectively, and just after the giant sawtooth crash at 7.1 sec are displayed.

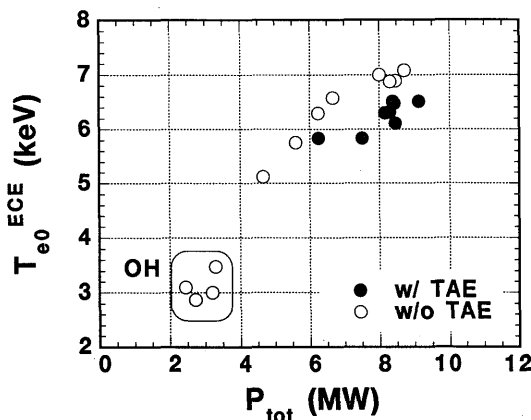


Fig. 23 The central electron temperature as a function of the total heating power. $^4\text{He} + (\text{H})$ discharges, $I_p = 3.5 \text{ MA}$, $q_{\text{eff}} = 3.2$, $\bar{n}_e = (2.1-2.6) \times 10^{19} \text{ m}^{-3}$ and $P_{\text{IC}} = (1.7-5.7) \text{ MW}$.

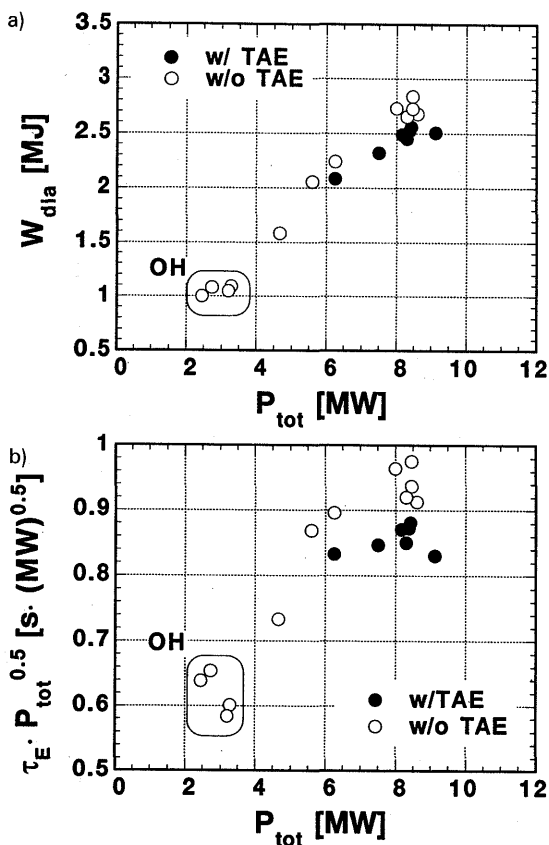


Fig. 24 (a) The diamagnetic stored energy as a function of the total heating power, for the same experimental conditions as in Fig. 23. (b) Corresponding normalized energy confinement time against the total heating power.

Figure 24 (a) indicates the diamagnetic stored energy against P_{tot} . The closed circles designate the case with TAE modes, while the open circles indicate the case where the TAE modes are suppressed just after the giant sawtooth crash. To illustrate the effect of TAE modes more clearly, we introduce a normalized energy confinement time ($\tau_E P_{tot}^{0.5}$), which is in proportion to the H-factor (τ_E / τ_E^{scal}), where we assume the power law scaling (i.e., $\tau_E^{scal} \propto P_{tot}^{-0.5}$) [32]. Figure 24 (b) indicates the normalized energy confinement time against P_{tot} , corresponding to the data in Fig. 24 (a). The sawtooth-stable period became longer than 0.6 sec (i.e., approximately $2 \times \tau_E$) for $P_{IC} > \sim 4$ MW (or $P_{tot} > \sim 6$ MW). Therefore, the normalized energy confinement time largely increases from the value of

the ohmic heating with increasing ICRF heating power until $P_{tot} \approx 6$ MW, and then tends to saturate. TAE modes appeared for $P_{tot} > \sim 6$ MW and the saturation is more clearly seen. However, the reduction of the normalized energy confinement time (H-factor) due to TAE modes is about 10% even at the highest power region. Thus, the impact of the TAE modes on the bulk plasma energy confinement is still moderate, possibly because the ICRF heating power is not so large, compared with the TAE threshold power.

5. Control of TAE Modes

5.1 Current Profile Control by Current Ramp

Effects of the plasma internal inductance, l_i , on TAE modes are investigated in view of control of TAE modes. In previous TAE mode experiments using tangential NBI heating on DIII-D [30] and TFTR [8], effects of change of l_i were explored by the current ramp technique. In DIII-D, it was found that TAE modes of lower toroidal mode numbers ($n=3-5$) are suppressed immediately after the current ramp-down (i.e., higher l_i). In TFTR, they found that TAE modes could be easily excited after current ramp-up (i.e., lower l_i) in otherwise difficult conditions for excitation of TAE modes. The explanation for these behaviours of TAE modes is that the continuum damping plays a dominant role in the damping mechanisms of TAE modes, because the continuum damping becomes stronger with increasing magnetic shear and vice versa [33]. In the case of current ramp-up/down experiments, the magnetic shear at the plasma edge is mainly modified. This is the reason why lower n modes, having broader mode structure, were suppressed after current ramp-down in DIII-D [30].

We first checked behaviours of TAE modes driven by ICRF heating in current ramp-up/down experiments. Figure 25 (a) and (b) show the examples of the current ramp up/down experiments. In Fig. 25 (a), the current was ramped up from 1.5 MA to 2 MA, resulting in decrease in l_i from 1.26 down to 0.86 before the ICRF heating. TAE modes appeared about 0.3 sec after starting ICRF injection. Their amplitudes decreased in time probably due to increase in l_i . The time evolution of the central electron temperature indicates only small sawtooth oscillation because of low l_i . On the other hand, in Fig. 25 (b), where the current was ramped down from 2.5 MA to 2 MA, resulting in increase in l_i from 1.08 up to 1.5, no TAE modes were

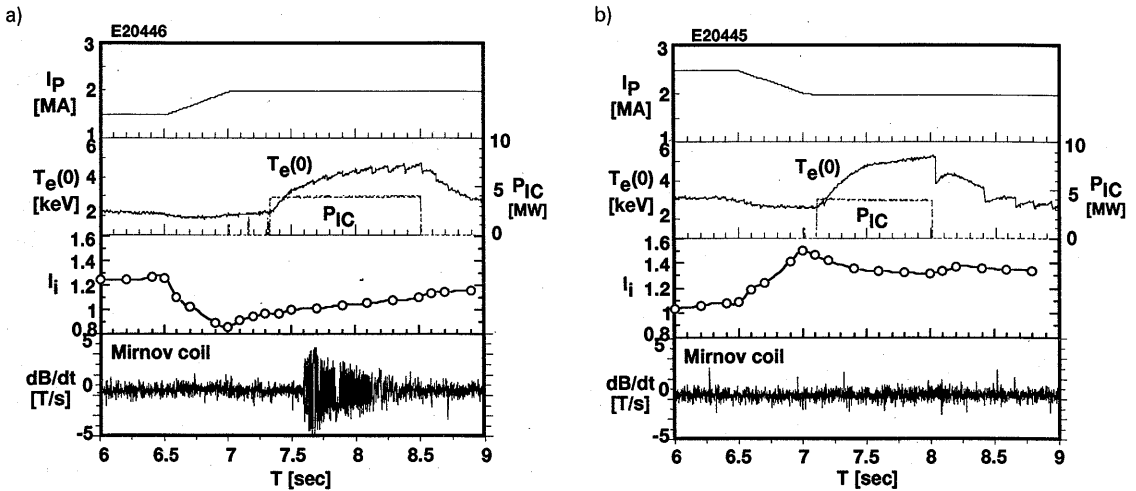


Fig. 25 Time evolution of TAE mode experiment with (a) current ramp-up and (b) current ramp-down before ICRF heating, showing the plasma current, the central electron temperature, the ICRF heating power, the internal inductance and the Mirnov coil signal. $\bar{n}_e = 2.3 \times 10^{19} \text{ m}^{-3}$ and $B_T = 3.8 \text{ T}$ in both cases.

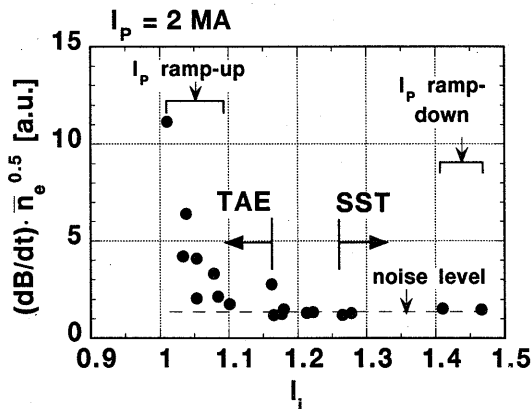


Fig. 26 Normalized TAE mode amplitudes measured by a Mirnov coil as a function of l_i with the inductive current drive. $\bar{n}_e = (1.8-2.6) \times 10^{19} \text{ m}^{-3}$ and $P_{IC} = (3.7-4) \text{ MW}$.

observed. A complete sawtooth stabilization during the ICRF heating took place in this case because the $q=1$ surface is relatively large after the current ramp-down, which is a necessary condition for the sawtooth stabilization by the second harmonic ICRF heating [34].

Figure 26 shows normalized TAE mode amplitudes measured by a Mirnov coil as a function of l_i for limited ranges of the ICRF power and the line average electron density, i.e., $P_{IC} = 3.7-4 \text{ MW}$ and $\bar{n}_e = 1.8-2.6 \times 10^{19} \text{ m}^{-3}$. The power range is close to the threshold power of TAE modes for normal operation

(i.e., $l_i \sim 1.2$). It is found that TAE amplitudes are greatly enhanced with decreasing l_i . Thus the control of TAE modes by the current ramp method was clearly confirmed in 2 MA discharges. It should also be noted that the domains of TAE modes and SST are clearly separated in terms of l_i .

5.2 Current Profile Control by LHCD

We then applied LHCD before ICRF injection to control TAE modes by non-inductive current profile control method for the first time [35]. Figure 27 shows the result, comparing two identical shots except for LHCD before ICRF injection (hereafter we call this 'pre-LHCD'). For LHCD, compound wave spectra (parallel refractive index $N_{||}$ of ~ 1.6 and ~ 2.3) of 3.1 MW total power were injected to reduce l_i efficiently [36]. Time evolution of l_i in Fig. 27 clearly indicates that an increasing rate of l_i is reduced with LHCD. Thereby, a value of l_i just before ICRF heating is by ~ 0.1 smaller with LHCD. As indicated in Fig. 27, TAE modes were observed during ICRF heating only for the case with pre-LHCD. Thus, the current profile control by such a non-inductive method of LHCD is also found to be effective to control TAE modes. At present, the current profile controllability of LHCD including increase in l_i is limited at low plasma current (1.2 MA), where excitation of TAE modes may be difficult because of confinement of MeV ions. However, opposite current drive [37] may be effective to

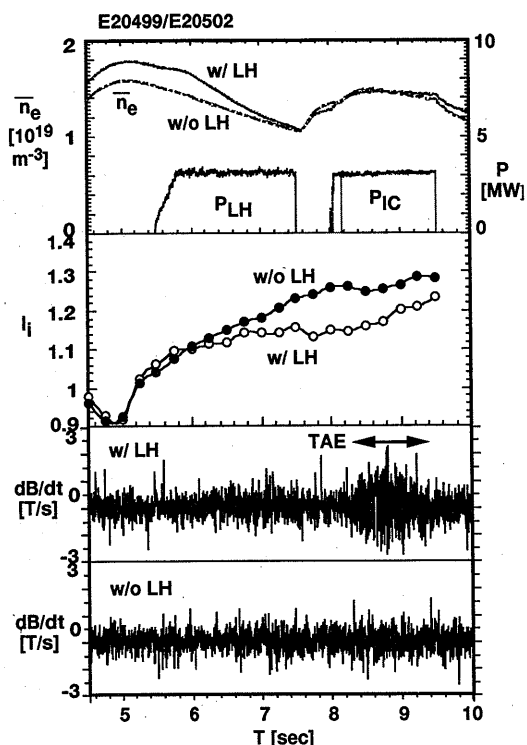


Fig. 27 Time evolution of TAE mode experiment with and without LHCD before ICRF heating, showing the line average electron density, the LHCD power, the ICRF heating power, the internal inductance, the Mirnov coil signals (dB/dt) with and without LHCD. $I_p=2$ MA and $B_T=3.8$ T.

increase I_i at high current regime (~ 3 MA) for suppression of TAE modes, which will be tested in near future.

5.3 Dependence on Internal Inductance

In Sec. 5.1 and Sec. 5.2, it is shown that both the current ramp method and the non-inductive current profile control method (pre-LHCD) are effective for control of TAE modes. In Fig. 28, quantities proportional to the tail ion stored energy (or beta because of the fixed toroidal field) are plotted against I_i including data of the current ramp and the pre-LHCD. Closed symbols indicate that TAE modes appeared. Open ones indicate absence of TAE modes. Horizontal arrows indicate time passing in the current ramp cases. It seems from the figure that the threshold beta value of the tail ion component tends to increase with increasing I_i . Note that the data with pre-LHCD show similar

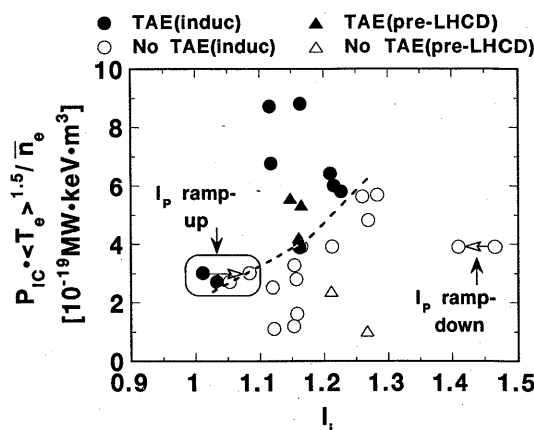


Fig. 28 $P_{IC} \cdot \langle T_e \rangle^{1.5} / \bar{n}_e$, which is proportional to the tail ion stored energy, as a function of the internal inductance. Circles designate the inductive current drive alone and triangles designate the pre-LHCD. Full symbols indicate that TAE modes appeared, while open symbols indicate no TAE modes appeared. $I_p=2$ MA, $B_T=3.8$ T, $\bar{n}_e=(1.3-3.3) \times 10^{19} \text{ m}^{-3}$, $P_{IC}=(1.4-4.3)$ MW and $P_{LH}=(1.7-3.1)$ MW.

behaviour to the other data of inductive current drive against I_i , although the current profiles may be different each other even for equal I_i . The results suggest that suppression of TAE modes by the non-inductive current profile control method is promising. However, the present experiments are limited at relatively low plasma current (2 MA). In high plasma current case ($I_p \geq 3$ MA), where higher-n modes tend to appear and the continuum damping becomes less important, we have had no systematic data on the I_i -dependence until now.

5.4 Effect of Sawtooth Relaxation

We observed that TAE modes disappear just after termination of the sawtooth stabilization (hereafter we call this a giant sawtooth crash) probably due to the loss of energetic ions. A typical example is shown in Fig. 14. At the same time with each sawtooth crash (7.10 sec, 8.04 sec and 8.74 sec), the coherent TAE modes disappear. After that, TAE modes are suppressed for 0.55–0.58 sec, resulting in increases in the diamagnetic stored energy and the central electron temperature from those of the first sawtooth-free period. Such a long suppression of TAE modes after a giant sawtooth crash is not simply due to the loss of

energetic ions, since neutron and γ -ray counts, which reflect MeV ions (see Sec. 4.1), exceed their maximum count in the first sawtooth-free period before TAE modes reappear in the second- and third-stable periods. One possible explanation is a change of the current profile after the giant sawtooth crash. A broader current density profile in the core, which may be produced after the giant sawtooth crash [23], gives higher local q -value and thus lower- n TAE modes, which is stable because of low fast ion growth rate. As the current density profile becomes more peaked during the reheating phase after the sawtooth crash, the q -value decreases and the toroidal mode number increases. The higher- n TAE modes can become unstable.

Thus, the current profile control in the plasma core is also useful for controlling TAE modes. In principle, if the safety factor in the core is limited in the range of $i-1/2n < q < i+1/2n$, ($i=1, 2, 3, \dots$), no Alfvén continuum gap exists there [17].

On the other hand, in the case of insufficient stabilization of sawtooth (i.e., shorter sawtooth repetition time case), we observed that TAE modes do not disappear at each sawtooth crash. This implies that energetic ions are not sensitive to the sawtooth crash with relatively small sawtooth inversion radius, possibly because of their large orbits.

6. Discussion and Conclusions

Characteristics of TAE modes driven by the second harmonic ICRF heating were widely explored in JT-60U, including the impacts on the fast ion and bulk plasma confinement and the control of TAE modes. A definite merit of TAE mode experiments by ICRF heating in JT-60U (or generally in present large tokamaks) is that MeV ions can be easily produced in the plasma core, resulting in making possible the excitation of TAE modes at the full toroidal field, for which the positive-ion NBI whose energy is around 100 keV cannot excite TAE modes. Thereby TAE mode behaviour in the high I_p and low- q regime, which is ITER relevant, could be explored. We observed important symptoms that higher n modes appear with increasing I_p (decreasing q_{eff}). In discharges of $I_p \geq 3.5$ MA, coherent TAE modes appear sequentially and their toroidal mode number increases one by one during a sawtooth free period. It is inferred that the toroidal mode number of at least 13 appeared. Furthermore, characteristic behaviour on the mode amplitudes, such that the mode

amplitudes increase exponentially with increasing n up to about 10 and then tend to saturate against n up to at least $n=13$. Analysis of these behaviours can give an important insight to prediction of TAE modes in ITER.

The threshold tail ion beta is found to be $\sim 0.05\%$ at $\bar{n}_e = (2.1-2.6) \times 10^{19} \text{ m}^{-3}$. However, relatively strong TAE modes were excited at $\bar{n}_e = 4.5 \times 10^{19} \text{ m}^{-3}$, where the tail ion beta is estimated to be at most $\sim 0.01\%$. It is inferred that higher n modes are excited at higher density.

Relations between TAE modes and ICRF heating conditions were elucidated. TAE modes are excited only for on-axis resonance, i.e., $|R_{\text{res}} - R_0|/a < 0.1$. In addition, asymmetry around the axis is found. TAE modes are excited more easily for low field side resonance. This is the same tendency as for the sawtooth stabilization. The result suggests that the deeply trapped ions play an important role in both phenomena. It appears that TAE modes are excited in the domain delimited by the $n_e n_H = \text{constant}$ line, where the second harmonic ICRF heating is efficient. Outside the domain, the heating becomes poor possibly because of the orbit effect and TAE modes cannot be excited.

Impacts of TAE modes were investigated mainly at high plasma current (3.5 MA). The reduction of the diamagnetic stored energy due to TAE modes is found to be dominated by the tail ion component. Reduction of the diamagnetic stored energy and the neutron counts due to TAE modes is in proportion to the TAE mode amplitudes measured by the Mirnov coil. The neutron counts reflect fast protons whose energy is higher than 3 MeV. The results suggest that the loss of fast ions due to TAE modes is mainly through resonant drift loss with the shear Alfvén waves [3]. The proportional coefficients decrease with increasing \bar{n}_e , linearly for the diamagnetic stored energy and exponentially for the neutron counts. This means that the loss of fast ions induced by TAE modes and associated degradation of the energy confinement becomes less important with increasing \bar{n}_e , since the resonant ion energy scales as $E_{\text{res}} \propto \bar{n}_e^{-1}$, although the TAE mode amplitudes are almost constant against \bar{n}_e above $\sim 2 \times 10^{19} \text{ m}^{-3}$. The electron temperature decreases only in the core region by onset of TAE modes. However, reduction of the central electron temperature and the energy confinement time is at most 1 keV and about

10%, respectively, at the present ICRF heating power level.

It is demonstrated that the current profile control by the non-inductive method using LHCD as well as the current ramp method is useful for control of TAE modes. By scanning I_1 in 2 MA discharges with the inductive current drive alone, the TAE domain and the SST domain are clearly separated with respect to I_1 . This is a favourable feature for obtaining high performance plasma, because the sawtooth stabilization and suppression of TAE modes are simultaneously achieved. The dependence of the threshold fast ion stored energy on I_1 is similar between the pre-LHCD case and the inductive drive case. This means that the current profile control by non-inductive current drive in the outer region may be powerful measures to suppress TAE modes in high- q discharges. It is also suggested that the current profile control in the plasma core is also effective for suppressing TAE modes, which was realized just after the giant sawtooth crash in low- q discharges.

In conclusion, the excitation and characteristics of high- n TAE modes, the impact on the fast ion and bulk plasma confinement, and the control of TAE modes by the non-inductive current drive have been demonstrated in JT-60U ICRF heating experiments.

Acknowledgments

We would like to express our appreciation to members of the JT-60U team, especially the ICRF operation team, for their support to this work. The authors are much indebted to Drs. C. Z. Cheng and G. Y. Fu for NOVA-K calculation and Dr. J. W. Van Dam for reading and criticizing the manuscript, in addition to valuable discussion and comments on TAE modes. Thanks are also due to Drs. R. Yoshino, V. I. Afanassiev, Y. Ikeda, Y. Kamada, Y. Koide, Y. Kusama, M. Nemoto, Y. Neyatani, T. Nishitani, M. Sato and K. Ushigusa for many helpful discussions. We also thank Drs. H. Kishimoto and M. Azumi for their support and encouragement.

References

- [1] C. Z. Cheng and M. S. Chance, *Phys. Fluids* **29**, 3695 (1986).
- [2] G. Y. Fu and J. W. Van Dam, *Phys. Fluids B* **1**, 1949 (1989).
- [3] D. J. Sigmar *et al.*, *Phys. Fluids B* **4**, 1506 (1992).
- [4] K. Tobita *et al.*, *Phys. Rev. Lett.* **69**, 3060 (1992).
- [5] K. L. Wong *et al.*, *Phys. Rev. Lett.* **66**, 1874 (1991).
- [6] W. W. Heidbrink *et al.*, *Nucl. Fusion* **31**, 1635 (1991).
- [7] J. R. Wilson *et al.*, *Proc. 14th Int. Conf. on Plasma Phys. and Controlled Nuclear Fusion Research* (Würzburg, 1992), IAEA, Vienna **1**, 661 (1993).
- [8] K. L. Wong *et al.*, *Plasma Phys. Control. Fusion* **36**, 879 (1994).
- [9] S. Ali-Arshad and D. J. Campbell, *Plasma Phys. Control. Fusion* **37**, 715 (1995).
- [10] M. Saigusa *et al.*, *Comprehensive Studies on Second Harmonic ICRF Heating in JT-60U*, *Proc. 15th Int. Conf. on Plasma Phys. and Controlled Nuclear Fusion Research* (Seville, 1994), paper IAEA-CN-60/A-3-I-5, to be published.
- [11] K. M. McGuire, *Recent D-T Results from TFTR*, *Proc. 4th IAEA Technical Committee Meeting and Joint US-Japan Workshop on Alpha Particles in Fusion Research* (Princeton, 1995), to be published.
- [12] G. Y. Fu, *Stability Analysis of TAE Modes in TFTR D-T Experiments*, *Proc. 4th IAEA Technical Committee Meeting and Joint US-Japan Workshop on Alpha Particles in Fusion Research* (Princeton, 1995), to be published.
- [13] A. Fasoli *et al.*, *Alfvén Eigenmodes Active Excitation Experiments in JET*, *Proc. 15th Int. Conf. on Plasma Phys. and Controlled Nuclear Fusion Research* (Seville, 1994), post-deadline paper, to be published.
- [14] P. Rebut, *The ITER EDA Outline Design*, *Proc. 15th Int. Conf. on Plasma Phys. and Controlled Nuclear Fusion Research* (Seville, 1994), paper IAEA/CN/60/E-1-I-1.
- [15] S. Putvinski, *et al.*, *Alpha-Particle Physics for ITER*, *Proc. 15th Int. Conf. on Plasma Phys. and Controlled Nuclear Fusion Research* (Seville, 1994), paper IAEA/CN/60/E-P-4.
- [16] H. Ninomiya *et al.*, *Phys. Fluids B* **4**, 2070 (1992).
- [17] M. Saigusa *et al.*, *Plasma Phys. Control. Fusion* **37**, 295 (1995).
- [18] H. Kimura *et al.*, *Physics Letters A* **199**, 86 (1995).
- [19] F. Porcelli *et al.*, *Plasma Phys. Controlled Fusion*

- 33, 1601 (1991).
- [20] M. Saigusa *et al.*, Nucl. Fusion **34**, 276 (1994).
- [21] T. Fujii *et al.*, Fusion Engineering and Design **26**, 377 (1995).
- [22] K. Ida *et al.*, Nucl. Fusion **31**, 943 (1991).
- [23] M. Sato *et al.*, *Estimation of Current Profile during ICRF Heated Discharges Characterized by Sawtooth Stabilization and Crash in JT-60U*, to be published in Jpn. J. Appl. Phys.
- [24] C. Z. Cheng, Phys. Report **211**, 1 (1992).
- [25] G. Y. Fu and C. Z. Cheng, *private communication*.
- [26] H. L. Berk *et al.*, Phys. Rev. Lett. **68**, 3563 (1992).
- [27] G. Y. Fu and W. Park, Phys. Rev. Lett. **74**, 1594 (1995).
- [28] H. Biglari *et al.*, Phys. Fluids B **4**, 2385 (1992).
- [29] G. Y. Fu and C. Z. Cheng, Phys. Fluids B **4**, 3722 (1992).
- [30] E. J. Strait *et al.*, Nucl. Fusion **33**, 1849 (1993).
- [31] H. Kimura *et al.*, Fusion Engineering and Design **26**, 95 (1995).
- [32] P. N. Yushmanov *et al.*, Nucl. Fusion **30**, 1999 (1990).
- [33] M. N. Rosenbluth *et al.*, Phys. Rev. Lett. **68**, 596 (1992).
- [34] H. Kimura *et al.*, *Proc. 10th Topical Conference on Radio Frequency Power in Plasmas*, (Boston, 1993), AIP, New York, 52 (1994).
- [35] M. Mori and the JT-60 Team, Plasma Phys. Controlled Fusion **36**, B181 (1994).
- [36] S. Ide *et al.*, Phys. Rev. Lett. **73**, 2312 (1994).
- [37] T. Kondoh *et al.*, *Proc. 21st EPS Conference on Controlled Fusion and Plasma Physics*, (Montpellier, 1994) Part III, 1138 (1994).